

Quasi-4-day Wave: Atmospheric Manifestation of the First Symmetric Rossby Normal Mode of Zonal Wavenumber 2

Y. Yamazaki¹, V. Matthias², Y. Miyoshi³

¹GFZ German Research Centre for Geosciences, Potsdam, Germany

²Deutsches Zentrum für Luft- und Raumfahrt, Institut für Solar-Terrestrische Physik, Neustrelitz, Germany

³Department of Earth and Planetary Sciences, Kyushu University, Fukuoka, Japan

Key Points:

- Climatology of westward-propagating quasi-4-day wave (Q4DW) with zonal wavenumber 2 is presented.
- Seasonal amplification is controlled by the critical layer and atmospheric instability.
- Arctic sudden stratospheric warmings can lead to an unseasonal enhancement of the wave.

Corresponding author: Yosuke Yamazaki, yamazaki@gfz-potsdam.de

This article has been accepted for publication and undergone full peer review but has not been through the copyediting, typesetting, pagination and proofreading process, which may lead to differences between this version and the [Version of Record](#). Please cite this article as doi: [10.1029/2021JD034855](https://doi.org/10.1029/2021JD034855).

This article is protected by copyright. All rights reserved.

Abstract

This paper describes global characteristics of the westward-propagating planetary wave with a period of ~ 4 days and zonal wavenumber 2, here referred to as quasi-4-day wave (Q4DW), which is considered to be a manifestation of the (2,1) Rossby normal mode. A climatology of the Q4DW is derived from geopotential height measurements by the Aura Microwave Limb Sounder during August 2004–December 2020. In the mesosphere and lower thermosphere (MLT), amplitude maxima occur at mid latitudes in May and August in the Northern Hemisphere, and in February and November in the Southern Hemisphere. With the amplitude exceeding 300 m, the Q4DW sometimes becomes the dominant mode of traveling planetary waves in the MLT. The seasonal variation is largely determined by the zonal mean state. As predicted by previous modeling work, the amplitude grows rapidly with height on the equatorward side of the critical layer, where the zonal mean flow is weakly eastward relative to the wave. The wave growth can be particularly large when there is a region of unstable mean flow across the boundary of the critical layer. This condition is met not only during the seasonal amplification of the Q4DW but also during some Arctic sudden stratospheric warming events, leading to an unseasonal enhancement.

1 Introduction

Classical wave theory utilizes the linearized equations governing atmospheric flow to describe properties of wave motions in the atmosphere (e.g. Lindzen & Chapman, 1969; Forbes, 1995). Under the assumption of a simplified atmosphere without dissipation and zonal mean winds, the linearized equations are separable in latitude and height. The latitude equation is known as Laplace’s tidal equation. The solutions to Laplace’s tidal equation are expressed in form of Hough functions, which give the latitudinal structure of waves. The height equation specifies the vertical structure of each Hough mode for given atmospheric forcing. In the absence of forcing, the assumption of an isothermal atmosphere with a rigid lower boundary (zero vertical velocity at the surface) leads to a single solution to Laplace’s tidal equation. The corresponding Hough functions represent free (unforced) oscillations or normal modes of the atmosphere.

The normal modes consist of gravity modes and Rossby modes. For an isothermal atmosphere with a temperature, say, $T=256\text{K}$ for the Earth, there is a series of westward-propagating Rossby normal modes that have a period longer than a day and shorter than several weeks (Kasahara, 1976; Salby, 1984; Madden, 2007; Sakazaki & Hamilton, 2020). These Rossby normal modes are thought to be responsible for, at least part of, multi-day oscillations commonly seen in atmospheric parameters. An individual Rossby normal mode is often expressed as $(s, n-s)$, where s is the zonal wavenumber and n is the meridional index. The oscillation is symmetric about the equator for an odd number of $n-s$ ($=1, 3, 5, \dots$) and antisymmetric for an even number of $n-s$ ($=2, 4, 6, \dots$). For example, (2,1) represents the first symmetric mode $n-s=1$ with zonal wavenumber $s=2$, and (1,2) represents the first asymmetric mode $n-s=2$ with zonal wavenumber 1. The predicted periods of Rossby normal modes include ~ 4 days for the (2,1) mode, ~ 5 days for the (1,1) mode, ~ 7 days for the (2,2) mode, ~ 10 days for the (1,2) mode, ~ 16 days for the (1,3) mode, ~ 28 days for the (1,4) mode. The vertical structure of Rossby normal modes is that of a Lamb wave. The phase of the wave is constant with height. Although the energy decreases exponentially in the vertical, the amplitude grows with height due to the reduction of the density.

In the presence of dissipation and nonuniform background fields, the phase is no longer constant with height, showing vertical propagation characteristics (Salby, 1981b, 1981a). Also, spectra of Rossby normal modes are suppressed, broadened, and shifted from those predicted by the classical theory (Kasahara, 1980; Salby & Roper, 1980; Salby, 1981b). Nonetheless, normal-mode-like oscillations, or quasi-normal modes, can exist in

67 a realistic atmosphere with latitudinal structures and periods similar to those of clas-
68 sical Rossby normal modes (Salby, 1981b, 1981a). Salby (1981b) numerically showed that
69 at least (1,1), (1,2), (1,3), (2,1) and (2,2) modes should be detectable as isolated spec-
70 tral signatures with the expected zonal wavenumbers. In fact, these modes have been
71 widely observed in the lower atmosphere (e.g., Madden, 1979, 2007; Sakazaki & Hamil-
72 ton, 2020). In the middle atmosphere, the latitude and height structures of Rossby nor-
73 mal modes are strongly influenced by the background atmosphere. Salby (1981a) pre-
74 sented a series of numerical experiments where the (2,1) mode response of the atmosphere
75 is examined under different background conditions. The results that are particularly rel-
76 evant to the present study are as follows:

- 77 1. The vertical growth rate of the wave is reduced in regions where the zonal mean
78 wind is strongly eastward relative to the wave.
- 79 2. Conversely, the growth rate is enhanced in regions where the zonal mean wind is
80 weakly eastward relative to the wave.
- 81 3. The wave cannot propagate across the critical layer, within which the zonal mean
82 wind is westward relative to the wave.
- 83 4. The enhancement and reduction of the growth rate occurs locally without affect-
84 ing other latitudes, thus introducing a hemispheric asymmetry.

85 As we will show later, the state of the zonal mean atmosphere largely determines the (2,1)
86 mode response in the mesosphere and lower thermosphere (MLT).

87 Quasi-normal mode oscillations in the middle atmosphere have been studied us-
88 ing global satellite data. Among others, the quasi-6-day wave (Q6DW), which is con-
89 sidered to be a manifestation of the (1,1) mode, is most extensively examined (e.g., Hi-
90 rota & Hirooka, 1984; Wu et al., 1994; Riggins et al., 2006; Forbes & Zhang, 2017; Qin
91 et al., 2021). Tropospheric processes are thought to be a source of the Q6DW (Miyoshi
92 & Hirooka, 1999). The wave can be amplified or locally excited in the middle atmosphere
93 through an instability of the zonal mean flow (Meyer & Forbes, 1997; Lieberman et al.,
94 2003; Liu et al., 2004; Gan et al., 2018). The Q6DW attains a large amplitude in the lower
95 thermosphere and its influence extends well into the ionosphere (Gu et al., 2014; Yamazaki
96 et al., 2018, 2020). Global features have also been studied for the quasi-10-day wave (Q10DW)
97 and quasi-16-day wave (Q16DW) in the middle atmosphere, which correspond to the (1,2)
98 and (1,3) modes, respectively (e.g., Hirooka & Hirota, 1985; Hirooka, 2000; Day & Mitchell,
99 2010; McDonald et al., 2011; Forbes & Zhang, 2015). Their sources, sinks, propagation
100 characteristics, and ionospheric effects are still to be established. Only few studies have
101 reported global observations of other normal modes in the middle atmosphere. Zhao et
102 al. (2019) observed a ~ 28 -day oscillation in the middle atmosphere and associated it with
103 the (1,4) mode. Hirota and Hirooka (1984) showed that westward-propagating ~ 4 -day
104 oscillations with zonal wavenumber 2 detected in the stratosphere are consistent with
105 the (2,1) mode. Ma et al. (2020) observed westward-propagating ~ 4 -day oscillations with
106 zonal wavenumber 2 in MLT temperature during the boreal winter in 2018/2019 and as-
107 sociated them with the (2,1) mode. The present study also focuses on westward-propagating
108 ~ 4 -day oscillations with zonal wavenumber 2 in the middle atmosphere. The oscillations
109 are regarded as a manifestation of the (2,1) Rossby normal mode, and we call them quasi-
110 4-day wave (Q4DW). It is noted that the term “4-day wave” has been sometimes used
111 to designate eastward-propagating ~ 4 -day oscillations with zonal wavenumber 1 in the
112 polar region (e.g., Randel & Lait, 1991; Allen et al., 1997; Lu et al., 2013). However, they
113 are not a Rossby normal mode, and thus should be distinguished from the Q4DW stud-
114 ied here.

115 As mentioned earlier, quasi-normal modes in the middle atmosphere are strongly
116 influenced by the zonal mean state of the atmosphere. The implication is that propa-
117 gation characteristics of quasi-normal modes may be altered when the background at-
118 mosphere undergoes significant changes, such as those during sudden stratospheric warm-

ings (SSW) (Andrews et al., 1987; Labitzke & Van Loon, 1999). The response of quasi-normal modes to SSW has been addressed in numerous studies (e.g., Hirooka & Hirota, 1985; Pancheva et al., 2008; Matthias et al., 2012; Sassi et al., 2012; Yu et al., 2019; Yamazaki & Matthias, 2019; He et al., 2020). These studies found that quasi-normal modes are sometimes enhanced around the time of SSW, but details of the response, such as the period of amplified wave and the timing of amplification relative to the SSW onset, can vary from event to event. The presence of the (2,1) mode has been noted during some SSW. For instance, Sassi et al. (2012) detected the Q4DW during the major SSW in January 2009, but not during other boreal winters (2004/2005, 2005/2006 and 2007/2008). Ma et al. (2020) presented observations of the Q4DW in mesospheric temperature, as well as ~ 4 -day oscillations in zonal and meridional winds at MLT altitudes, during the major SSW in 2018/2019. They suspected that the baroclinic/barotropic instability might be responsible for the amplification of the Q4DW. Baroclinically and barotropically unstable regions arise from large vertical and horizontal shears of the zonal wind, respectively. The unstable regions can provide a source of energy for the enhancement of a wave, and are considered to be important for seasonal and unseasonal enhancements of quasi-normal modes. The role of the baroclinic/barotropic instability has been particularly well studied for the Q6DW (e.g., Liu et al., 2004). The relationship between the baroclinic/barotropic instability and Q4DW activity is yet to be established.

The main objectives of this study are (1) to determine the global seasonal climatology of the Q4DW, (2) to examine the relationship between the seasonal variations of the Q4DW and background atmosphere, and (3) to explore the link between the Q4DW and SSW based on long-term global observations. To this end, we use 16 years of geopotential height and temperature measurements from the Microwave Limb Sounder (MLS) onboard NASA's Aura satellite (Waters et al., 2006). Detailed descriptions of the data and method of the analysis are provided in the following section.

2 Data and Method of Analysis

The primary data employed in this study are geopotential height measurements from Aura/MLS during August 2004–December 2020 (Waters et al., 2006; Schwartz et al., 2008). The data cover the pressure levels from 261 to 0.001 hPa, which correspond roughly to 9 and 97 km, respectively. We use the log-pressure height $z = H \ln(p_0/p)$ to approximate the height of the measurements, where H ($=7$ km) is the scale height, p_0 ($=1013.25$ hPa) is the sea level pressure, and p is the pressure. The method for evaluating wave components is the same as that used in Yamazaki and Matthias (2019). The amplitude A and phase ϕ of a wave with zonal wavenumber s and period τ were determined by fitting of the following formula to the data collected at a given latitude and height:

$$\sum_{s=-4}^4 A_{s,\tau} \cos \left[2\pi \left(\frac{t}{\tau} + s\lambda \right) - \phi_{s,\tau} \right], \quad (1)$$

where t is the universal time, and λ is the longitude. In this definition, $s < 0$ and $s > 0$ corresponds respectively to eastward- and westward-propagating waves, and $s = 0$ represents a zonally symmetric oscillation. The least-squares fitting was performed using a time window that is 3 times the wave period and a latitude window of $\pm 5^\circ$. Before the fitting, the data were separated into those obtained in the ascending and descending portions of the orbit, and for each group of the data, the mean value was subtracted. The residuals in both groups were used in the fitting. In this way, aliasing from migrating solar tides can be avoided (Meek & Manson, 2009). Signatures of migrating solar tides are stationary in both ascending and descending parts of the orbit, as the Aura spacecraft is in a Sun-synchronous orbit. Signatures of tidal modulation by planetary waves could still alias into the derived signatures of planetary waves because of limited spatial and temporal coverage of the data, but in general, atmospheric perturbations associated with tidal modulation are very small below 100 km (Gan et al., 2017; Miyoshi & Yamazaki, 2020).

Geostrophic winds were derived from the geopotential height measurements using the method described in Matthias and Ern (2018). The zonal mean zonal wind \bar{u}_g was used to identify the critical layer, where the mean flow relative to the wave is westward:

$$\bar{u}_g - C_{s,\tau} < 0. \quad (2)$$

Here $C_{s,\tau}$ is the phase velocity of a wave with zonal wavenumber s and period τ . At latitude ϕ ,

$$C_{s,\tau} = -\frac{2\pi a}{s\tau} \cos \phi \quad (3)$$

where a ($= 6.37 \times 10^6$ m) is the Earth's radius.

An instability of the mean flow is evaluated by the potential vorticity gradient, \bar{q}_y , defined by

$$\bar{q}_y = \frac{2\Omega}{a} \cos \phi - \frac{1}{a^2} \frac{\partial}{\partial \phi} \left[\frac{1}{\cos \phi} \frac{\partial}{\partial \phi} (\bar{u}_g \cos \phi) \right] - \frac{1}{\rho} \frac{\partial}{\partial z} \left(\rho \frac{f^2}{N^2} \frac{\partial \bar{u}_g}{\partial z} \right), \quad (4)$$

where Ω ($= 7.292 \times 10^{-5}$ rad s $^{-1}$) is the rotation rate of the Earth, ρ is the atmospheric density, f ($= 2\Omega \sin \phi$) is the Coriolis frequency, and N is the buoyancy frequency. The density is derived based on the ideal gas law using temperature measurements by Aura/MLS. The buoyancy frequency is derived from Aura/MLS temperature profiles:

$$N^2 = \frac{g}{T} \left(\frac{\partial T}{\partial z} + \frac{g}{c_p} \right), \quad (5)$$

where g is the gravitational acceleration, T is the atmospheric temperature and c_p ($= 1004$ J K $^{-1}$ kg $^{-1}$) is the specific heat of dry air. A necessary condition for the baroclinic/barotropic instability is $\bar{q}_y < 0$. In regions where $\bar{q}_y < 0$, the mean flow is unstable to perturbations, and a wave can amplify by extracting energy from the unstable mean flow.

3 Results and Discussion

3.1 Seasonal climatology of the quasi-4-day wave

Here we present the seasonal climatology of the Q4DW derived from the long-term record of Aura/MLS geopotential height during August 2004–December 2020. Figure 1 displays westward-propagating wave spectra for zonal wavenumber $s=2$ (W2) and $s=1$ (W1) at 0.001 hPa (97 km) at mid-latitudes. The W2 component shows a well-defined seasonal pattern in both the Northern and Southern Hemispheres. In the Northern Hemisphere, enhanced W2 wave activity with periods around 4 days are seen in May and August, while in the Southern Hemisphere, similar wave activity is seen in February and November. The results suggest that the Q4DW is the predominant W2 component in the mid-latitude MLT. The mean period of the Q4DW is 3.8 ± 0.4 days, which is close to the predicted period of the (2,1) mode, e.g., 3.84 days according to Madden (2007). The spectral peak around 4 days is also observed at other altitudes in the lower thermosphere and upper mesosphere (not shown here). However, in the lower mesosphere and below (say, < 65 km), the ~ 4 -day peak is usually not resolved.

The results for the W1 component suggest that the Q6DW is predominant at this height, which is in agreement with previous studies (e.g., Qin et al., 2021). The maximum amplitude of the Q6DW (~ 250 m) is greater than that of the Q4DW (~ 180 m). For W1, the period of the dominant wave tends to be shorter during local summer and longer during local winter. This is owing to the fact that the zonal mean zonal wind is more westward during local summer in large part of the middle atmosphere (20–90 km), as shown in the third panels. Since shorter-period waves have larger phase speed, they are more likely to reach higher altitudes without encountering the critical layer during local summer. The period of the dominant W2 wave seems to show a similar seasonal

214 pattern, but the amplitude is small during the local winter, so that it is difficult to de-
 215 termine the period.

216 The bottom panels of Figure 1 show the meridional structures of the Q4DW and
 217 Q6DW at a height of 97 km. The Q4DW amplitude is defined here as the maximum am-
 218 plitude of W2 waves with a period between 3–5 days. Similarly, the Q6DW amplitude
 219 is defined as the maximum amplitude of W1 waves with a period between 4.5–7 days.
 220 At 97 km, amplitude maxima occur about $\pm 45^\circ$ latitudes for both the Q4DW and Q6DW.
 221 The mid-latitude maxima in geopotential height perturbations are consistent with the
 222 meridional structures of the (2,1) and (1,1) modes, which are indicated by the white dashed
 223 curves.

224 The vertical structure of the climatological mean Q4DW is depicted in Figure 2
 225 for February 11, May 17, August 11 and November 15, when the amplitude is relatively
 226 large in the MLT. The gray lines in the figure indicate the boundary of the critical layer.
 227 That is, the zonal mean wind relative to the wave is westward in areas poleward of the
 228 lines. As mentioned earlier, the Q4DW cannot propagate across the critical layer. It is
 229 seen that the Q4DW grows rapidly in the vertical near the equatorward boundary of the
 230 critical layer, which is consistent with the numerical results by Salby (1981a). Magenta
 231 colored areas in Figure 2 indicate regions where the necessary condition for the baroclinic/barotropic
 232 instability is met, i.e., $\bar{q}_y < 0$. In all cases, there is an unstable region around the criti-
 233 cal layer, at altitudes of 50–70 km. Thus, it is possible that the Q4DW is amplified or
 234 locally excited in the mesopause region.

235 Figure 3 shows the vertical structure of the climatological mean Q4DW in equinox
 236 and solstice conditions, when the amplitude is relatively small. During the equinoxes,
 237 unstable regions ($\bar{q}_y < 0$) are seen at high latitudes but there is no critical layer, around
 238 which the wave can rapidly grow. During the solstices, a critical layer is seen in the sum-
 239 mer hemisphere. However, unlike the times of the seasonal amplification of the Q4DW
 240 presented in Figure 2, unstable regions with $\bar{q}_y < 0$ are confined inside the critical layer
 241 and do not extend beyond its boundary. Thus, the wave cannot be amplified or locally
 242 excited in the unstable regions.

243 Figure 4 gives an overview of the Q4DW events in 16 August 2012 and 11 Novem-
 244 ber 2014, where the amplitude was particularly large. The top panels show that the Q4DW,
 245 with the amplitude greater than 300 m, was the dominant component of traveling plan-
 246 etary waves in the MLT in both cases. The amplitude structures, presented in the mid-
 247 dle panels, are similar to those in the climatological results (Figure 2) but the amplitudes
 248 are much larger. The vertical and meridional distributions of the phase are shown in the
 249 bottom panels. At altitudes above 50 km or so, downward phase progression with height
 250 is seen, indicating upward energy propagation. The vertical wavelength in the MLT, as
 251 estimated by fitting a linear regression to the phase values above 60 km, is approximately
 252 58 km at 45°N for the August 2012 event, and 69 km at 45°S for the November 2014 event.
 253 These values are comparable with the typical vertical wavelength of the Q6DW, e.g., 60–
 254 70 km as reported by Forbes and Zhang (2017). The phase is largely symmetric about
 255 the equator, which is consistent with the classical (2,1) mode.

256 It is noted that there is considerable year-to-year variability in the magnitude of
 257 the seasonal enhancement of the Q4DW. This can be seen in Figure 5 for the Northern
 258 Hemisphere. Figure 5 shows the amplitude of the Q4DW at 45°N during 2005–2020. En-
 259 hanced Q4DW activity is seen in May and August, but the maximum amplitude varies
 260 from year to year. We checked distributions of unstable regions ($\bar{q}_y < 0$) and their rela-
 261 tionship to the critical layer, but did not find a systematic difference in their patterns
 262 between the years with relatively large and small seasonal enhancements of the Q4DW.
 263 The results suggest that the consideration of the critical layer and atmospheric insta-
 264 bility alone is not sufficient to explain the year-to-year variability of the Q4DW. A pos-

sible explanation is the propagation of the Q4DW from the lower atmosphere, which could vary from year to year.

3.2 Quasi-4-day wave event during sudden stratospheric warmings

In Figure 5, enhanced wave activity is occasionally seen in the mesosphere during boreal winters. Such an unseasonal enhancement of the Q4DW is not observed in the Southern Hemisphere (not shown here). The bursts of Q4DW activity in the Northern Hemisphere during winter coincide with major SSW, which are also indicated in Figure 5. Examples of such are the SSW in January 2009, January 2013, February 2018 and January 2019. The response is particularly prominent during the January 2009 and January 2019 events. Below we examine the W2 response to SSW in more detail. The response of the W1 component to SSW is presented in Yamazaki and Matthias (2019) and thus will not be considered here.

Figure 6 depicts the W2 response to the SSW in January 2009 and January 2019, when the Q4DW response is most pronounced. A rapid increase in the polar stratospheric temperature (top panels), together with the reversal of the zonal mean zonal wind (middle panels), indicates the occurrence of SSW. The January 2009 event (left panels) is one of the strongest major warmings in the record (e.g., Manney et al., 2009; Harada et al., 2010) and its whole atmosphere impact has been extensively studied (e.g., Jin et al., 2012; Pedatella et al., 2014). According to Aura/MLS geostrophic winds, the reversal of the zonal wind at 32 km and 60°N occurred on 24 January 2009. At 64 km, enhanced wave activity in the W2 component is observed at a period of ~ 5 days around 22–26 January and ~ 4 days around 27–31 January. The January 2019 event is another major warming (e.g., Rao et al., 2019) but the middle atmosphere response is not as pronounced as that during the January 2009 event. The wind reversal at 32 km was recorded on 31 December 2018. Strong wave activity is in the W2 component at a period ~ 4 days around 30 December 2018–2 January 2019.

In Figure 6, enhanced W2 wave activity is also seen at a period of ~ 7 days during both the SSW, which may be related to the first asymmetric mode of zonal wavenumber 2, or the (2,2) mode. Largest ~ 7 -day oscillations are observed at $\sim 50^\circ\text{N}$ (not shown here), which is consistent with the (2,2) mode. The expected antisymmetric phase structure was, however, not detected, as the waves are mostly confined to the Northern Hemisphere and it was difficult to determine the phase in the Southern Hemisphere.

Figure 7 shows the W2 response to major warming events in January 2013 (left panels) and February 2018 (right panels). For the January 2013 event, the wind reversal at 32 km occurred on 7 January 2013, and enhanced wave activity in the W2 component at periods 4–5 days is observed at 64 km around 5–13 January 2013. For the February 2018 event, the wind reversal took place on 12 February 2018. Although W2 wave activity during this SSW was not as strong as that during the other SSW mentioned above, a minor burst of ~ 4 -day wave activity was observed around 16–20 February 2018.

Figure 8 compares the height structures of the Q4DW before SSW (left panels), during SSW (middle panels) and after SSW (right panels) for the events, from the top to the bottom, in the boreal winters of 2008/2009, 2018/2019, 2012/2013, 2017/2018 and 2005/2006. The central date assigned as “during SSW” is 30 January 2009 for the 2008/2009 event, 1 January 2019 for the 2018/2019 event, 13 January 2013 for the 2012/2013 event, 13 February 2018 for the 2017/2018 event, and 25 January 2006 for the 2005/2006 event. The dates 20 days before and after the central dates are assigned as “before SSW” and “after SSW”, respectively.

Before SSW (left panels), the distributions of the critical layer and unstable mean flow are similar to the climatological pattern for the December solstice presented in Figure 3. That is, a critical layer exists in the Southern Hemisphere at mesospheric heights,

315 within which unstable regions with $\bar{q}_y < 0$ are confined. During SSW (middle panels), an
316 additional critical layer appears in the Northern Hemisphere high-latitude region, and
317 a region of unstable mean flow extends beyond the critical layer. The formation of the
318 critical layer and unstable region in the Northern Hemisphere is a direct result of the zonal
319 wind reversal connected to SSW. As discussed earlier in the context of the seasonal am-
320 plification of the Q4DW (Figure 2), an unstable region extending across the boundary
321 of the critical layer gives a favorable condition for vertical growth of the Q4DW. After
322 SSW (right panels), the state of the background atmosphere is different depending on
323 the event. No critical layer is seen after the January 2009 and February 2018 events, and
324 overall Q4DW activity is low, similar to the equinox cases (Figure 3). After the 2018/2019
325 event, the background atmosphere went back to the December solstice type, with the crit-
326 ical layer in the Southern Hemisphere encompassing an unstable region, and thus there
327 is no Q4DW enhancement. After the January 2006 and 2013 events, the Q4DW in the
328 Southern Hemisphere MLT is enhanced, as the critical layer moves to higher latitudes
329 and an unstable region extends across the boundary of the critical layer, which repre-
330 sents typical February conditions (Figure 2).

331 A difference between Q4DW enhancement during SSW and seasonal Q4DW en-
332 hancement is that during SSW, the wave amplification occurs at lower heights than dur-
333 ing times of seasonal enhancement. This can be understood from the fact that during
334 periods of seasonal enhancement, the critical layer and unstable regions appear in the
335 mesosphere (50–80 km), while they are mainly in the stratosphere (20–50 km) during
336 SSW. Figure 9 shows the vertical growth rate of the Q4DW amplitude during the Jan-
337 uary 2009 and 2019 SSW (top panels). Largest wave growth is observed at 40–50 km,
338 where the zonal wind relative to the wave is reduced. At MLT altitudes, the zonal wind
339 is strongly eastward relative to the wave, which prevents vertical growth of the wave. Dur-
340 ing seasonal enhancement of the Q4DW (bottom panels), on the other hand, largest wave
341 growth occurs in the MLT, as the zonal wind is weakly eastward relative to the wave.

342 The previous study by Ma et al. (2020) reported enhanced Q4DW activity in the
343 MLT during the 2018/2019 SSW. They suspected that the barotropic/baroclinic insta-
344 bility might be the source of the wave. Our results support this possibility. We also put
345 emphasis on the presence of the critical layer, around which the vertical growth rate of
346 quasi-normal modes are predicted to increase (Salby, 1981a). Gu et al. (2018) pointed
347 out that changes in the distributions of the critical layer and unstable regions can ex-
348 plain the response of the quasi-2-day wave (a manifestation of mixed Rossby-gravity wave)
349 to the SSW in January 2006. A similar concept is used here to understand the behav-
350 ior of the Q4DW during SSW events. Sassi et al. (2012), examining quasi-normal modes
351 in the middle atmosphere during SSW, noted that the Q4DW was present during the
352 January 2009 event but not during other SSW in 2006 and 2008. We have confirmed their
353 findings. Q4DW activity was strong during the SSW in January 2009 and 2019. Enhanced
354 but weaker wave activity was detected during the SSW in January 2013 and February
355 2018. For other years, it was difficult to identify wave activity associated with the Q4DW,
356 including the major warming in January 2006.

357 It remains unclear why some SSW are accompanied by stronger Q4DW activity
358 than others. Properties of SSW depend on various factors, including the SSW type, quasi-
359 biennial oscillation (QBO) phase, and solar flux (e.g., Charlton & Polvani, 2007; Camp
360 & Tung, 2007), and accordingly, the wave response to SSW can also vary depending on
361 them (Pogoreltsev et al., 2014; Siddiqui et al., 2018). An SSW can be classified into wave-
362 1 and wave-2 types, which are driven by enhanced planetary wave forcing with zonal wavenum-
363 ber 1 and 2, respectively. Wave-1 and wave-2 types are generally associated with the dis-
364 placement and splitting of the polar vortex. Figure 10 shows daily amplitudes of wave-
365 1 and wave-2 components of the planetary wave at 10 hPa (32 km) and 60°N during each
366 SSW, as determined by the Fourier analysis of Aura/MLS geopotential height data (solid
367 line) as well as the corresponding data from the NCEP-DOE Reanalysis 2 (Kanamitsu

et al., 2002) (dashed line). Choi et al. (2019) introduced a simple method to distinguish between wave-1 and wave-2 types. That is, if the wave-2 amplitude exceeds the wave-1 amplitude on any day during ± 10 days from the reversal of the zonal mean zonal wind, the event is said to be wave-2 type; otherwise, it is called wave-1 type. Based on this definition, the February 2007, January 2009, January 2013, and February 2018 SSW are wave-2 type and the rest is wave-1 type. Although the January 2019 event is classified here as wave-1 type, Rao et al. (2019) pointed out that this SSW was neither typical wave-1 nor wave-2 type, involving complex forcing from waves 1–3 following the SSW onset. They observed split of the polar vortex in synoptic charts of the 10hPa heights starting around 4–8 January 2019. This is after peak activity of the Q4DW, and thus the vortex split during the January 2019 SSW is unlikely involved in the Q4DW enhancement. The vertical green lines in Figure 10 indicate the central date of Q4DW events. In summary, there is no apparent correlation between the occurrence of Q4DW enhancement during SSW and the type of the SSW. Also, Q4DW enhancement during SSW is observed under both easterly and westerly phases of the QBO, regardless of the solar flux level. The QBO phase, determined by the equatorial zonal mean zonal wind at 50 hPa from the NCEP-DOE Reanalysis 2, is indicated in Figure 10 for each SSW, along with the solar flux index $F_{10.7}$ (Tapping, 2013).

4 Summary and Conclusions

Aura/MLS geopotential height data have been used to examine the westward-propagating ~ 4 -day wave with zonal wavenumber 2, or quasi-4-day wave (Q4DW), in the middle atmosphere, which is regarded as a manifestation of the (2,1) Rossby normal mode in the presence of dissipation and nonuniform background. The seasonal climatology of the Q4DW is obtained from the data during August 2004–December 2020. The main results may be summarized as follows:

1. Geopotential height perturbations of the Q4DW in the mesosphere and lower thermosphere (MLT) are largest at middle latitudes, approximately $\pm 45^\circ$ latitudes, reflecting the meridional structure of the classical (2,1) mode.
2. Seasonal amplification of the Q4DW in the MLT occurs in May and August in the Northern Hemisphere, and in February and November in the Southern Hemisphere. The mean period of the Q4DW is 3.8 ± 0.4 days.
3. The Q4DW amplitude is generally smaller than that of the quasi-6-day wave (Q6DW), which is a manifestation of the (1,1) Rossby normal mode. Nevertheless, the Q4DW occasionally becomes the predominant component of traveling planetary waves in the MLT with the geopotential height amplitude exceeding 300 m.
4. The phase is symmetric about the equator, which is consistent with the (2,1) mode. At MLT altitudes, the vertical structure of the phase shows downward progression with height, with the vertical wavelength of approximately 60–70 km. The downward phase propagation is consistent with the quasi-normal mode behavior under the presence of dissipation and nonuniform background fields.
5. The seasonal variation of the Q4DW in the MLT can be explained in terms of background conditions. During the seasonal enhancement of the Q4DW, the vertical growth of the wave is increased near the critical layer as predicted by the modeling work by Salby (1981a). At the same time, an unstable region ($\bar{q}_y < 0$) extends across the boundary of the critical layer, where the wave can be amplified or locally excited by extracting energy from the unstable mean flow.
6. During the equinoxes, the Q4DW amplitude in the MLT is small, as there is no critical layer. During the solstices, the critical layer exists in the summer hemisphere, but the Q4DW amplitude is not as large as that during May, August, February and November, as unstable regions with $\bar{q}_y < 0$ are confined within the critical layer.

- 419 7. In addition to the seasonal amplification, the Q4DW sometimes attains a large am-
 420 plitude in the MLT during times of Arctic sudden stratospheric warmings (SSW).
 421 This can be explained by the distributions of the critical layer and unstable mean
 422 flow, in a similar way as the seasonal amplification. Q4DW enhancement is ob-
 423 served during both wave-1 and wave-2 types of SSW, regardless of the quasi-biennial
 424 oscillation phase and solar flux level.

425 This study has established that the Q4DW is an important part of atmospheric variabil-
 426 ity at MLT heights. The seasonal amplification of the Q4DW is a robust feature, but the
 427 extent of the amplification varies from year to year. Similarly, the extent of the Q4DW
 428 amplification during SSW also varies from event to event. More studies are needed to
 429 understand the mechanism for these variabilities. Also, a broader impact of the Q4DW
 430 on the ionosphere/thermosphere system still needs to be assessed in future work.

431 Acknowledgments

432 We thank the NASA Goddard Earth Sciences (GES) Data and Information Services Cen-
 433 ter (DISC) (<https://disc.gsfc.nasa.gov/>) for making the Aura/MLS geopotential
 434 height data (DOI: 10.5067/Aura/MLS/DATA2008) available. This work was supported
 435 in part by JSPS and DFG (grant YA-574-3-1) under the Joint Research Projects-LEAD
 436 with DFG.

437 References

- 438 Allen, D., Stanford, J., Elson, L., Fishbein, E., Froidevaux, L., & Waters, J. (1997).
 439 The 4-day wave as observed from the upper atmosphere research satellite
 440 microwave limb sounder. *Journal of the atmospheric sciences*, *54*(3), 420–434.
 441 Andrews, D. G., Leovy, C. B., & Holton, J. R. (1987). *Middle atmosphere dynamics*
 442 (Vol. 40). Academic press.
 443 Camp, C. D., & Tung, K.-K. (2007). The influence of the solar cycle and qbo on
 444 the late-winter stratospheric polar vortex. *Journal of the atmospheric sciences*,
 445 *64*(4), 1267–1283.
 446 Charlton, A. J., & Polvani, L. M. (2007). A new look at stratospheric sudden warm-
 447 ings. part i: Climatology and modeling benchmarks. *Journal of climate*, *20*(3),
 448 449–469.
 449 Choi, H., Kim, B.-M., & Choi, W. (2019). Type classification of sudden strato-
 450 spheric warming based on pre-and postwarming periods. *Journal of climate*,
 451 *32*(8), 2349–2367.
 452 Day, K., & Mitchell, N. (2010). The 16-day wave in the arctic and antarctic meso-
 453 sphere and lower thermosphere. *Atmospheric Chemistry and Physics*, *10*(3),
 454 1461–1472.
 455 Forbes, J. M. (1995). Tidal and planetary waves. *The Upper Mesosphere and Lower*
 456 *Thermosphere: A Review of Experiment and Theory, Geophys. Monogr. Ser.*,
 457 *87*, 67–87.
 458 Forbes, J. M., & Zhang, X. (2015). Quasi-10-day wave in the atmosphere. *Journal of*
 459 *Geophysical Research: Atmospheres*, *120*(21), 11–079.
 460 Forbes, J. M., & Zhang, X. (2017). The quasi-6 day wave and its interactions with
 461 solar tides. *Journal of Geophysical Research: Space Physics*, *122*(4), 4764–
 462 4776.
 463 Gan, Q., Oberheide, J., & Pedatella, N. M. (2018). Sources, sinks, and propagation
 464 characteristics of the quasi 6-day wave and its impact on the residual mean cir-
 465 culation. *Journal of Geophysical Research: Atmospheres*, *123*(17), 9152–9170.
 466 Gan, Q., Oberheide, J., Yue, J., & Wang, W. (2017). Short-term variability in
 467 the ionosphere due to the nonlinear interaction between the 6 day wave and
 468 migrating tides. *Journal of Geophysical Research: Space Physics*, *122*(8),

- 8831–8846.
- 469 Gu, S.-Y., Dou, X., Pancheva, D., Yi, W., & Chen, T. (2018). Investigation of the
470 abnormal quasi 2-day wave activities during the sudden stratospheric warm-
471 ing period of january 2006. *Journal of Geophysical Research: Space Physics*,
472 *123*(7), 6031–6041.
- 473 Gu, S.-Y., Liu, H.-L., Li, T., Dou, X., Wu, Q., & Russell III, J. M. (2014). Observa-
474 tion of the neutral-ion coupling through 6 day planetary wave. *Journal of Geo-
475 physical Research: Space Physics*, *119*(12), 10–376.
- 476 Harada, Y., Goto, A., Hasegawa, H., Fujikawa, N., Naoe, H., & Hirooka, T. (2010).
477 A major stratospheric sudden warming event in january 2009. *Journal of the
478 Atmospheric Sciences*, *67*(6), 2052–2069.
- 479 He, M., Yamazaki, Y., Hoffmann, P., Hall, C. M., Tsutsumi, M., Li, G., & Chau,
480 J. L. (2020). Zonal wave number diagnosis of rossby wave-like oscillations
481 using paired ground-based radars. *Journal of Geophysical Research: Atmo-
482 spheres*, *125*(12), e2019JD031599.
- 483 Hirooka, T. (2000). Normal mode rossby waves as revealed by UARS/ISAMS obser-
484 vations. *Journal of Atmospheric Sciences*, *57*(9), 1277–1285.
- 485 Hirooka, T., & Hirota, I. (1985). Normal mode rossby waves observed in the upper
486 stratosphere. Part II: Second antisymmetric and symmetric modes of zonal
487 wavenumbers 1 and 2. *Journal of Atmospheric Sciences*, *42*(6), 536–548.
- 488 Hirota, I., & Hirooka, T. (1984). Normal mode rossby waves observed in the upper
489 stratosphere. Part I: First symmetric modes of zonal wavenumbers 1 and 2.
490 *Journal of Atmospheric Sciences*, *41*(8), 1253–1267.
- 491 Jin, H., Miyoshi, Y., Pancheva, D., Mukhtarov, P., Fujiwara, H., & Shinagawa, H.
492 (2012). Response of migrating tides to the stratospheric sudden warming
493 in 2009 and their effects on the ionosphere studied by a whole atmosphere-
494 ionosphere model gaia with cosmic and timed/saber observations. *Journal of
495 Geophysical Research: Space Physics*, *117*(A10).
- 496 Kanamitsu, M., Ebisuzaki, W., Woollen, J., Yang, S.-K., Hnilo, J., Fiorino, M., &
497 Potter, G. (2002). NCEP–DOE AMIP-II Reanalysis (R-2). *Bulletin of the
498 American Meteorological Society*, *83*(11), 1631–1644.
- 499 Kasahara, A. (1976). Normal modes of ultralong waves in the atmosphere. *Monthly
500 Weather Review*, *104*(6), 669–690.
- 501 Kasahara, A. (1980). Effect of zonal flows on the free oscillations of a barotropic at-
502 mosphere. *Journal of the Atmospheric Sciences*, *37*(5), 917–929.
- 503 Labitzke, K., & Van Loon, H. (1999). *The stratosphere: phenomena, history, and
504 relevance*. Springer Science & Business Media.
- 505 Lieberman, R., Riggin, D., Franke, S., Manson, A., Meek, C., Nakamura, T., ...
506 Reid, I. (2003). The 6.5-day wave in the mesosphere and lower thermosphere:
507 Evidence for baroclinic/barotropic instability. *Journal of Geophysical Research:
508 Atmospheres*, *108*(D20).
- 509 Lindzen, R. S., & Chapman, S. (1969). Atmospheric tides. *Space science reviews*,
510 *10*(1), 3–188.
- 511 Liu, H.-L., Talaat, E., Roble, R., Lieberman, R., Riggin, D., & Yee, J.-H. (2004).
512 The 6.5-day wave and its seasonal variability in the middle and upper atmo-
513 sphere. *Journal of Geophysical Research: Atmospheres*, *109*(D21).
- 514 Lu, X., Chu, X., Fuller-Rowell, T., Chang, L., Fong, W., & Yu, Z. (2013). Eastward
515 propagating planetary waves with periods of 1–5 days in the winter antarctic
516 stratosphere as revealed by merra and lidar. *Journal of Geophysical Research:
517 Atmospheres*, *118*(17), 9565–9578.
- 518 Ma, Z., Gong, Y., Zhang, S., Zhou, Q., Huang, C., Huang, K., ... Li, G. (2020).
519 Study of a quasi 4-day oscillation during the 2018/2019 ssw over mohe, china.
520 *Journal of Geophysical Research: Space Physics*, *125*(7), e2019JA027687.
- 521 Madden, R. A. (2007). Large-scale, free rossby waves in the atmospherean update.
522 *Tellus A: Dynamic Meteorology and Oceanography*, *59*(5), 571–590.
- 523

- 524 Manney, G. L., Schwartz, M. J., Krüger, K., Santee, M. L., Pawson, S., Lee, J. N.,
 525 ... Livesey, N. J. (2009). Aura microwave limb sounder observations of dy-
 526 namics and transport during the record-breaking 2009 arctic stratospheric
 527 major warming. *Geophysical Research Letters*, *36*(12).
- 528 Matthias, V., & Ern, M. (2018). On the origin of the mesospheric quasi-stationary
 529 planetary waves in the unusual arctic winter 2015/2016. *Atmospheric chem-
 530 istry and physics*, *18*(7), 4803–4815.
- 531 Matthias, V., Hoffmann, P., Rapp, M., & Baumgarten, G. (2012). Composite
 532 analysis of the temporal development of waves in the polar mlt region during
 533 stratospheric warmings. *Journal of atmospheric and solar-terrestrial physics*,
 534 *90*, 86–96.
- 535 McDonald, A., Hibbins, R. E., & Jarvis, M. J. (2011). Properties of the quasi 16 day
 536 wave derived from eos mls observations. *Journal of Geophysical Research: At-
 537 mospheres*, *116*(D6).
- 538 Meek, C., & Manson, A. (2009). Summer planetary-scale oscillations: aura mls
 539 temperature compared with ground-based radar wind. In *Annales geophysicae*
 540 (Vol. 27, pp. 1763–1774).
- 541 Meyer, C. K., & Forbes, J. M. (1997). A 6.5-day westward propagating planetary
 542 wave: Origin and characteristics. *Journal of Geophysical Research: Atmo-
 543 spheres*, *102*(D22), 26173–26178.
- 544 Miyoshi, Y., & Hirooka, T. (1999). A numerical experiment of excitation of the 5-
 545 day wave by a gcm. *Journal of the atmospheric sciences*, *56*(11), 1698–1707.
- 546 Miyoshi, Y., & Yamazaki, Y. (2020). Excitation mechanism of ionospheric 6-day os-
 547 cillation during the 2019 september sudden stratospheric warming event. *Jour-
 548 nal of Geophysical Research: Space Physics*, *125*(9), e2020JA028283.
- 549 Pancheva, D., Mukhtarov, P., Mitchell, N., Merzlyakov, E., Smith, A., Andonov,
 550 B., ... others (2008). Planetary waves in coupling the stratosphere and
 551 mesosphere during the major stratospheric warming in 2003/2004. *Journal of
 552 Geophysical Research: Atmospheres*, *113*(D12).
- 553 Pedatella, N., Fuller-Rowell, T., Wang, H., Jin, H., Miyoshi, Y., Fujiwara, H., ...
 554 others (2014). The neutral dynamics during the 2009 sudden stratosphere
 555 warming simulated by different whole atmosphere models. *Journal of Geophys-
 556 ical Research: Space Physics*, *119*(2), 1306–1324.
- 557 Pogoreltsev, A., Savenkova, E., & Pertsev, N. (2014). Sudden stratospheric warm-
 558 ings: the role of normal atmospheric modes. *Geomagnetism and Aeronomy*,
 559 *54*(3), 357–372.
- 560 Qin, Y., Gu, S.-Y., Teng, C.-K.-M., Dou, X.-K., Yu, Y., & Li, N. (2021). Com-
 561 prehensive study of the climatology of the quasi-6-day wave in the mlt region
 562 based on aura/mls observations and sd-waccm-x simulations. *Journal of Geo-
 563 physical Research: Space Physics*, e2020JA028454.
- 564 Randel, W. J., & Lait, L. R. (1991). Dynamics of the 4-day wave in the south-
 565 ern hemisphere polar stratosphere. *Journal of Atmospheric Sciences*, *48*(23),
 566 2496–2508.
- 567 Rao, J., Garfinkel, C. I., Chen, H., & White, I. P. (2019). The 2019 new year strato-
 568 spheric sudden warming and its real-time predictions in multiple S2S models.
 569 *Journal of Geophysical Research: Atmospheres*, *124*(21), 11155–11174.
- 570 Riggins, D. M., Liu, H.-L., Lieberman, R. S., Roble, R. G., Russell Iii, J. M.,
 571 Mertens, C. J., ... others (2006). Observations of the 5-day wave in the meso-
 572 sphere and lower thermosphere. *Journal of Atmospheric and Solar-Terrestrial
 573 Physics*, *68*(3-5), 323–339.
- 574 Sakazaki, T., & Hamilton, K. (2020). An array of ringing global free modes discov-
 575 ered in tropical surface pressure data. *Journal of Atmospheric Sciences*, *77*(7),
 576 2519–2539.
- 577 Salby, M. L. (1981a). Rossby normal modes in nonuniform background configura-
 578 tions. Part 1: Simple fields. *Journal of the Atmospheric Sciences*, *38*(9), 1803–

- 579 1826.
- 580 Salby, M. L. (1981b). Rossby normal modes in nonuniform background configura-
581 tions. Part 2: Equinox and solstice conditions. *Journal of the Atmospheric Sci-*
582 *ences*, 38(9), 1827–1840.
- 583 Salby, M. L. (1984). Survey of planetary-scale traveling waves: The state of theory
584 and observations. *Reviews of Geophysics*, 22(2), 209–236.
- 585 Salby, M. L., & Roper, R. (1980). Long-period oscillations in the meteor region.
586 *Journal of the Atmospheric Sciences*, 37(1), 237–244.
- 587 Sassi, F., Garcia, R., & Hoppel, K. (2012). Large-scale rossby normal modes dur-
588 ing some recent northern hemisphere winters. *Journal of the Atmospheric Sci-*
589 *ences*, 69(3), 820–839.
- 590 Schwartz, M., Lambert, A., Manney, G., Read, W., Livesey, N., Froidevaux, L., ...
591 others (2008). Validation of the aura microwave limb sounder temperature
592 and geopotential height measurements. *Journal of Geophysical Research:*
593 *Atmospheres*, 113(D15).
- 594 Siddiqui, T. A., Yamazaki, Y., Stolle, C., Lühr, H., Matzka, J., Maute, A., & Pe-
595 datella, N. (2018). Dependence of lunar tide of the equatorial electrojet on
596 the wintertime polar vortex, solar flux, and qbo. *Geophysical Research Letters*,
597 45(9), 3801–3810.
- 598 Tapping, K. (2013). The 10.7 cm solar radio flux ($F_{10.7}$). *Space Weather*, 11(7),
599 394–406.
- 600 Wang, H., Boyd, J. P., & Akmaev, R. A. (2016). On computation of hough func-
601 tions. *Geoscientific Model Development*, 9(4), 1477–1488.
- 602 Waters, J. W., Froidevaux, L., Harwood, R. S., Jarnot, R. F., Pickett, H. M., Read,
603 W. G., ... others (2006). The earth observing system microwave limb sounder
604 (eos mls) on the aura satellite. *IEEE Transactions on Geoscience and Remote*
605 *Sensing*, 44(5), 1075–1092.
- 606 Wu, D., Hays, P., & Skinner, W. (1994). Observations of the 5-day wave in the
607 mesosphere and lower thermosphere. *Geophysical Research Letters*, 21(24),
608 2733–2736.
- 609 Yamazaki, Y., & Matthias, V. (2019). Large-amplitude quasi-10-day waves in the
610 middle atmosphere during final warmings. *Journal of Geophysical Research:*
611 *Atmospheres*, 124(17-18), 9874–9892.
- 612 Yamazaki, Y., Matthias, V., Miyoshi, Y., Stolle, C., Siddiqui, T., Kervalishvili, G.,
613 ... others (2020). September 2019 antarctic sudden stratospheric warming:
614 Quasi-6-day wave burst and ionospheric effects. *Geophysical Research Letters*,
615 47(1), e2019GL086577.
- 616 Yamazaki, Y., Stolle, C., Matzka, J., & Alken, P. (2018). Quasi-6-day wave mod-
617 ulation of the equatorial electrojet. *Journal of Geophysical Research: Space*
618 *Physics*, 123(5), 4094–4109.
- 619 Yu, F. R., Huang, K. M., Zhang, S. D., Huang, C. M., Yi, F., Gong, Y., ... Ning,
620 B. (2019). Quasi 10-and 16-day wave activities observed through meteor radar
621 and mst radar during stratospheric final warming in 2015 spring. *Journal of*
622 *Geophysical Research: Atmospheres*, 124(12), 6040–6056.
- 623 Zhao, Y., Taylor, M. J., Pautet, P.-D., Moffat-Griffin, T., Hervig, M. E., Murphy,
624 D. J., ... Russell III, J. (2019). Investigating an unusually large 28-day
625 oscillation in mesospheric temperature over antarctica using ground-based
626 and satellite measurements. *Journal of Geophysical Research: Atmospheres*,
627 124(15), 8576–8593.

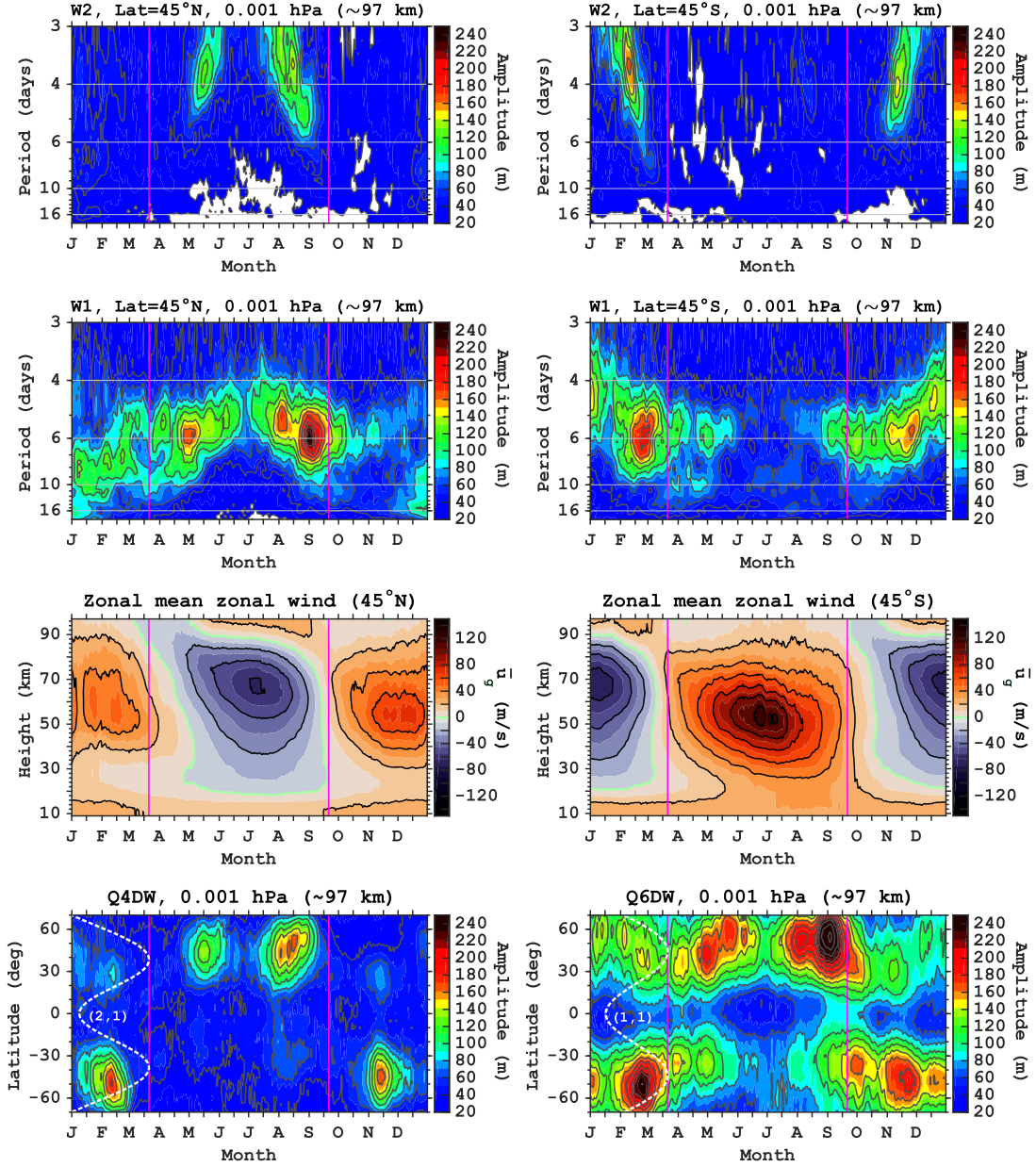


Figure 1. Spectra of Aura/MLS geopotential height at 0.001 hPa (97 km) during August 2004–December 2020. The top panels show month versus period distributions for the westward-propagating zonal wavenumber 2 (W2) component at 45°N (left) and 45°S (right), while the second panels are for the westward-propagating zonal wavenumber 1 (W1) component. The third panels show the zonal mean zonal wind at 45°N (left) and 45°S (right), as derived from Aura/MLS geostrophic winds. The bottom panels show month versus latitude distributions the amplitude of the quasi-4-day wave (Q4DW) (left) and quasi-6-day wave (Q6DW) (right). The maximum amplitude of the W2 component at periods 3–5 days is taken as the Q4DW amplitude, while the maximum amplitude of the W1 component at periods 4.5–7 days is taken as the Q6DW amplitude. The meridional structures of the (2,1) Rossby normal mode and (1,1) Rossby normal mode are indicated by the white dashed curves. These Hough functions are computed using the code given by Wang et al. (2016). In all panels, the vertical magenta lines correspond to the equinoxes.

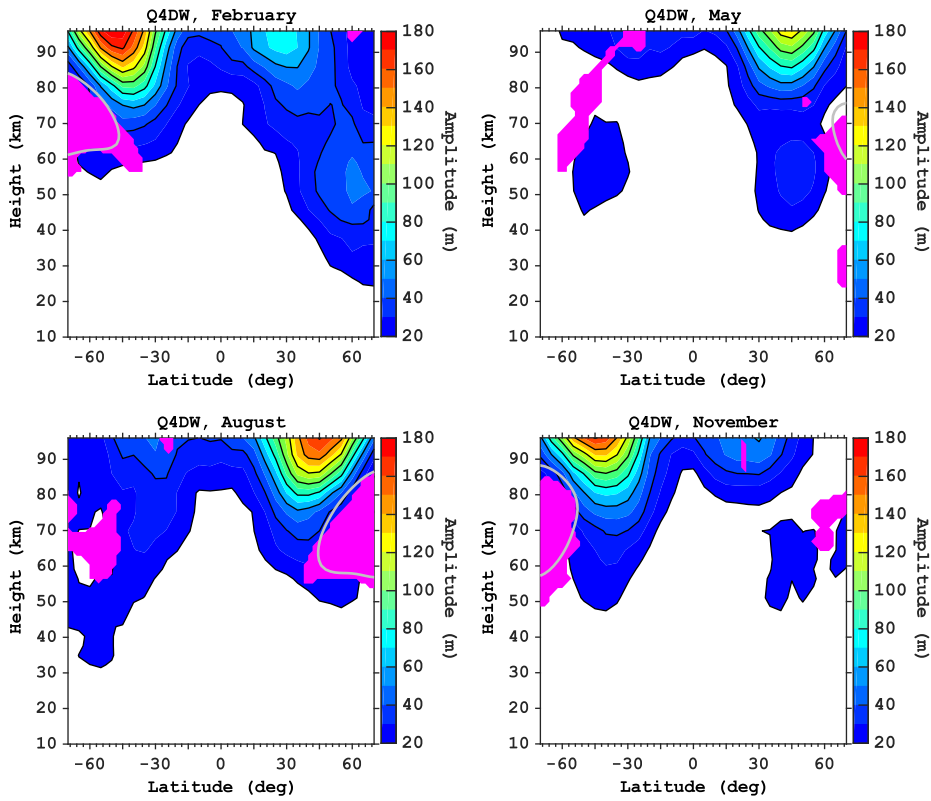


Figure 2. Latitude versus height distributions of the amplitude of the quasi-4-day wave (Q4DW) for 11 February (top left), 17 May (top right), 11 August (bottom left) and 15 November (bottom right). They are climatological representations based on the average of 16 years of the Aura/MLS geopotential height observations. The gray lines indicate the boundary of the critical layer for the Q4DW. The magenta shading indicates regions of unstable zonal mean flow ($\bar{q}_y < 0$).

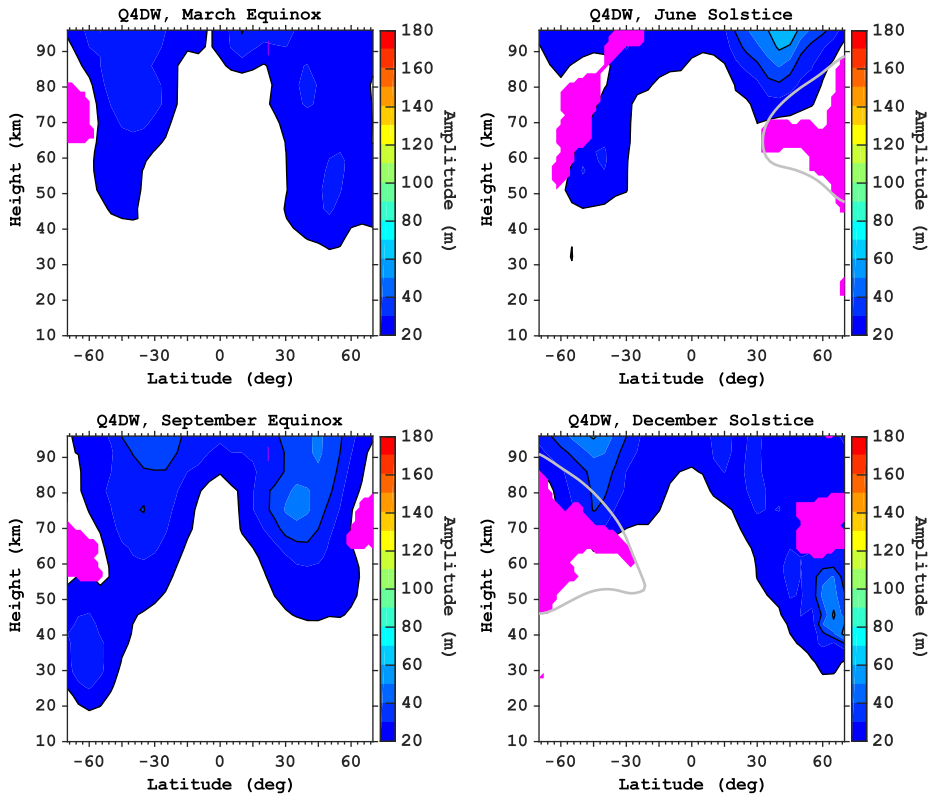


Figure 3. Latitude versus height distributions of the amplitude of the quasi-4-day wave (Q4DW) for 21 March (top left), 21 June (top right), 21 September (bottom left) and 21 December (bottom right). They are climatological representations based on the average of 16 years of the Aura/MLS geopotential height observations. The gray lines indicate the boundary of the critical layer for the Q4DW. The magenta shading indicates regions of unstable zonal mean flow ($\bar{q}_y < 0$).

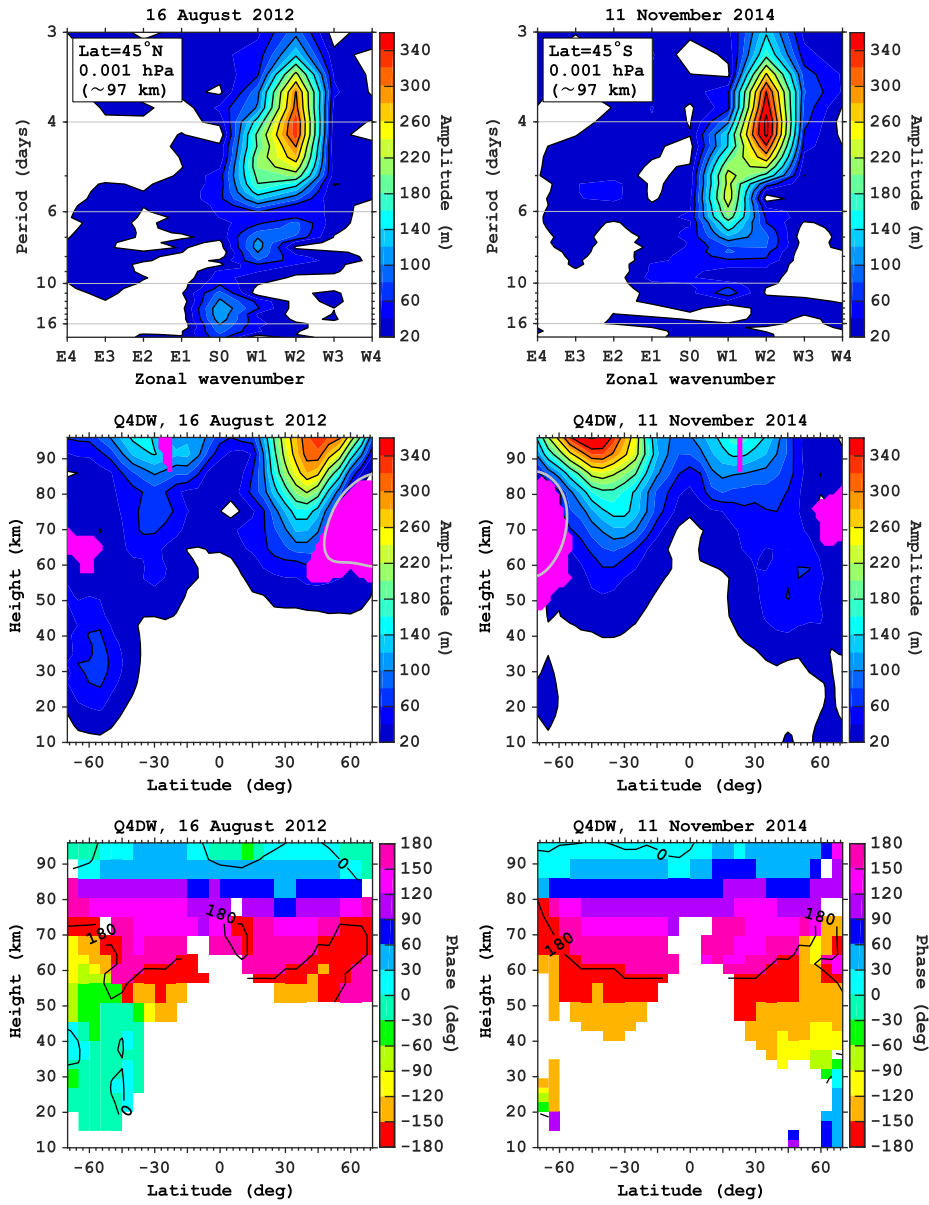


Figure 4. Overview of large-amplitude quasi-4-day wave (Q4DW) events in 16 August 2012 (left) and 11 November 2014 (right). (Top) Zonal wavenumber versus period spectra of Aura/MLS geopotential height at 0.001 hPa (97 km). (Middle) Latitude versus height distributions of the Q4DW amplitude. The gray lines indicate the boundary of the critical layer for the Q4DW. The magenta shading indicates regions of unstable zonal mean flow ($\bar{q}_y < 0$). (Bottom) Latitude versus height distributions of the Q4DW phase.

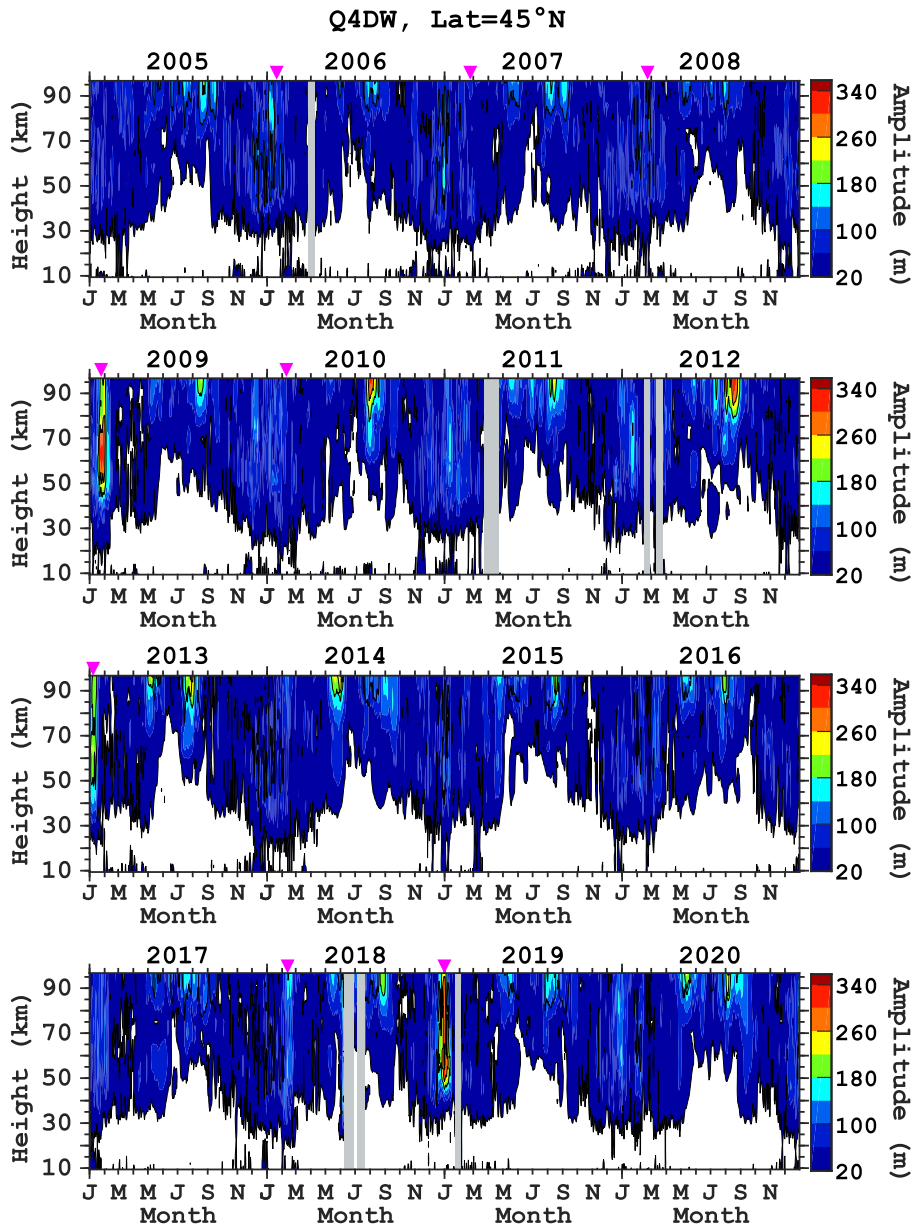


Figure 5. Month versus height plots for the amplitude of the quasi-4-day wave (Q4DW) in Aura/MLS geopotential height at 45°N from 2005 to 2020. The onset times of the zonal mean zonal wind reversal at 10 hPa (32 km) and 60°N associated with major sudden stratospheric warmings (SSW) are indicated by downward arrows. The identification of the wind reversal is based on Aura/MLS geostrophic winds.

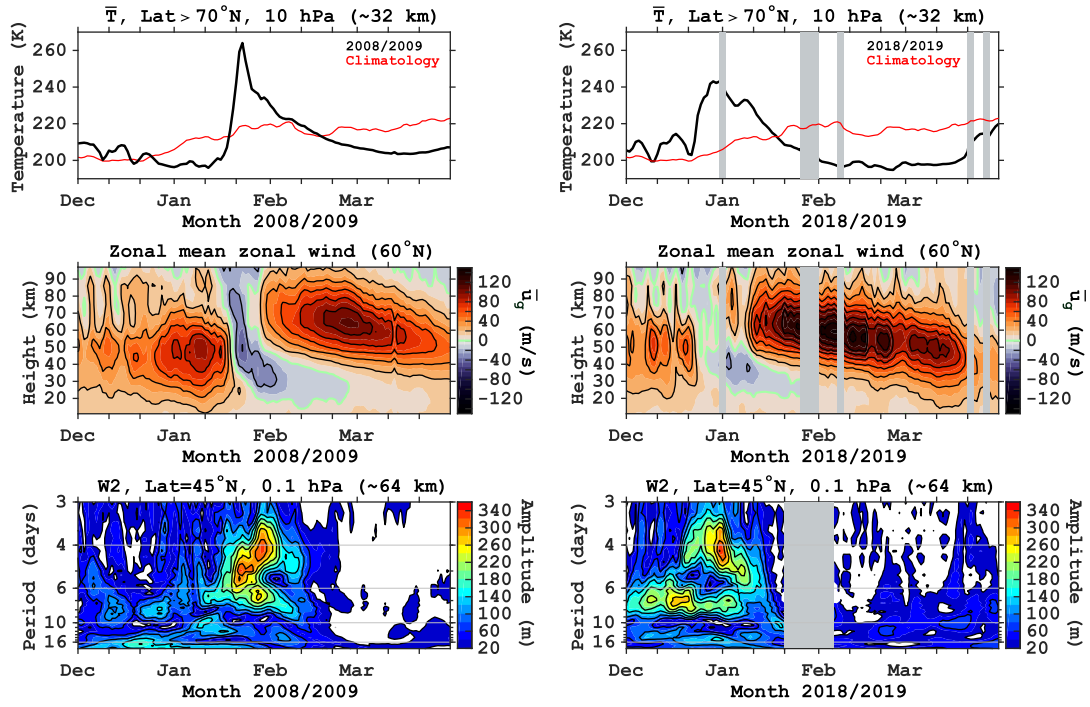


Figure 6. Sudden stratospheric warmings in the boreal winters of 2008/2009 (left) and 2018/2019 (right). The top panels show time series of Aura/MLS temperature at 10 hPa (32 km) averaged above 70°N (black) and the corresponding climatological seasonal cycle during 2004–2020 (red). The middle panels show month versus height plots of the zonal mean zonal wind at 60°N. The bottom panels show month versus period spectra of Aura/MLS geopotential height at 0.1 hPa (64 km) for the westward-propagating zonal wavenumber 2 (W2) component.

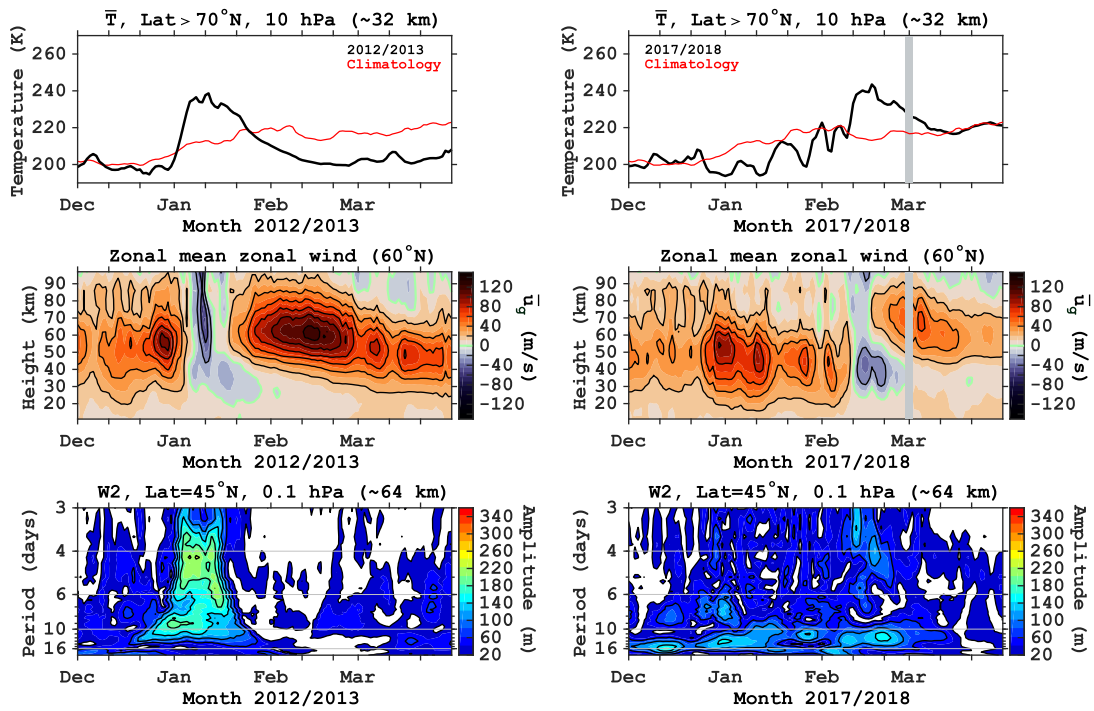


Figure 7. Same as Figure 6 but for sudden stratospheric warmings in the boreal winters of 2012/2013 (left) and 2017/2018 (right).

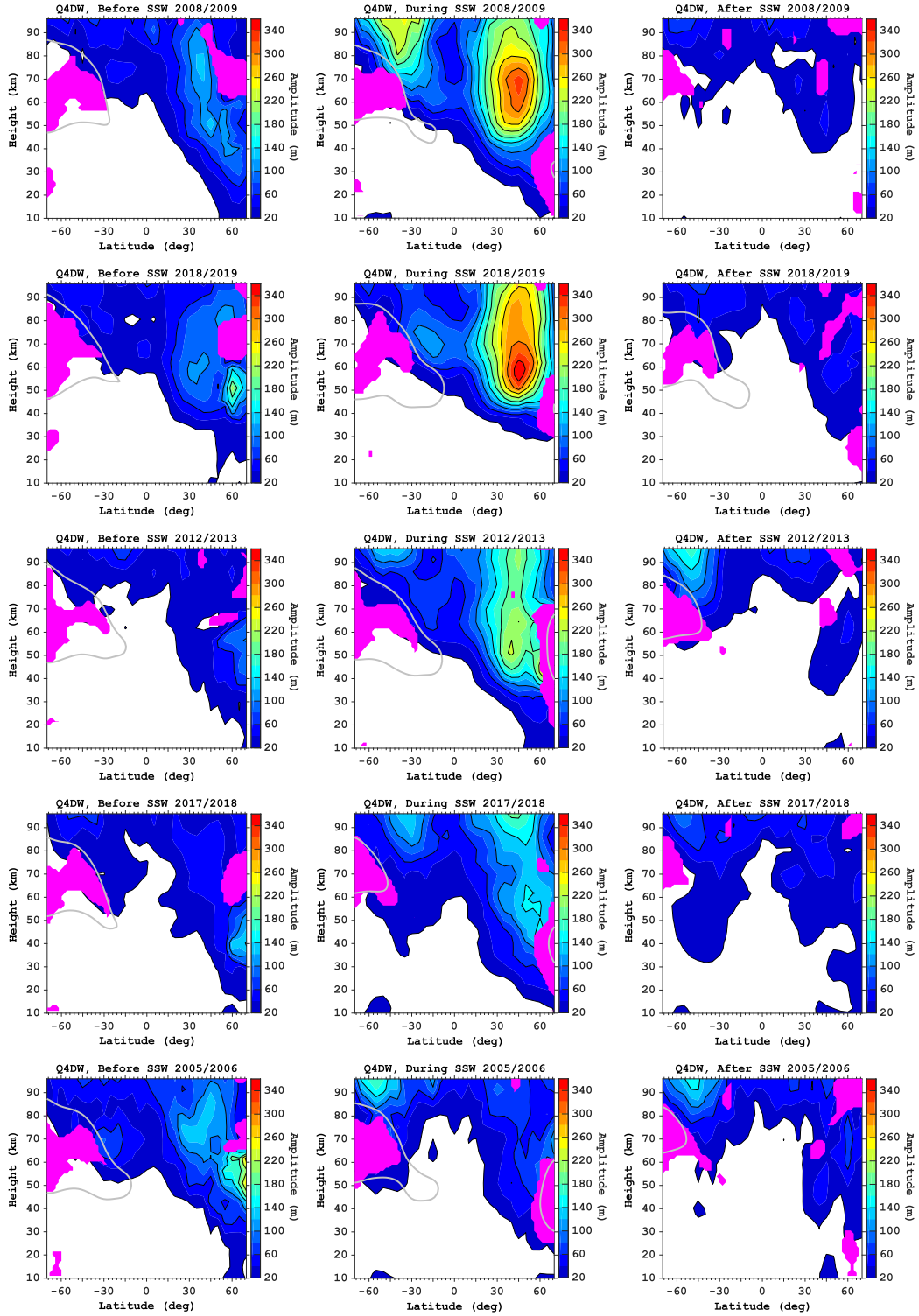


Figure 8. Latitude versus height distributions of the quasi-4-day wave (Q4DW) amplitude during sudden stratospheric warmings (SSW) in the boreal winters of, from the top to the bottom, 2008/2009, 2018/2019, 2012/2013, 2017/2018 and 2005/2006. The central date for each event is 30 January 2009, 1 January 2019, 13 January 2013, 13 February 2018 and 25 January 2006. For comparisons, the results are also presented for 20 days before (left) and after (right) the central dates. The gray lines indicate the boundary of the critical layer for the Q4DW. The magenta shading indicates regions of unstable zonal mean flow ($\bar{q}_y < 0$).

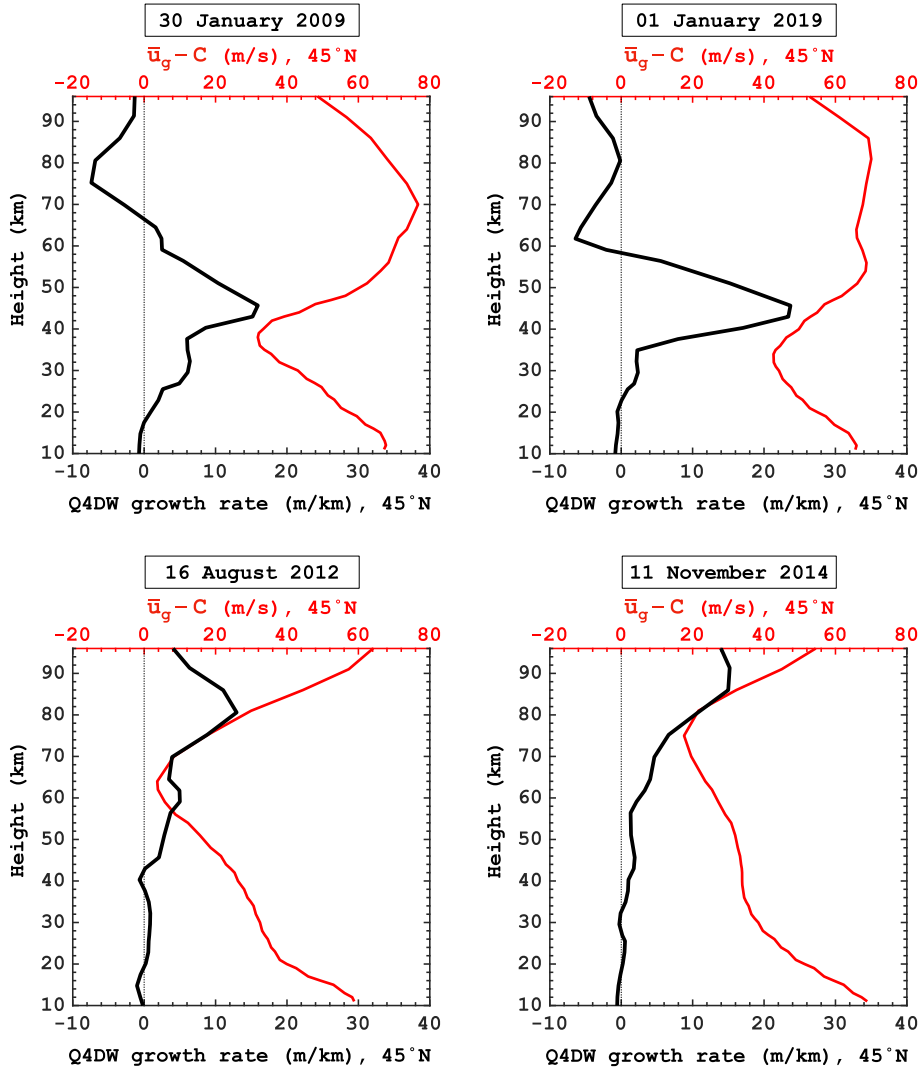


Figure 9. Vertical growth rate of the quasi-4-day wave (Q4DW) at 45°N for 30 January 2009 (upper left), 1 January 2019 (upper right), 16 August 2012 (lower left) and 11 November 2014 (lower right). The red curves indicate the zonal mean zonal wind velocity at 45°N relative to the phase speed of the Q4DW.

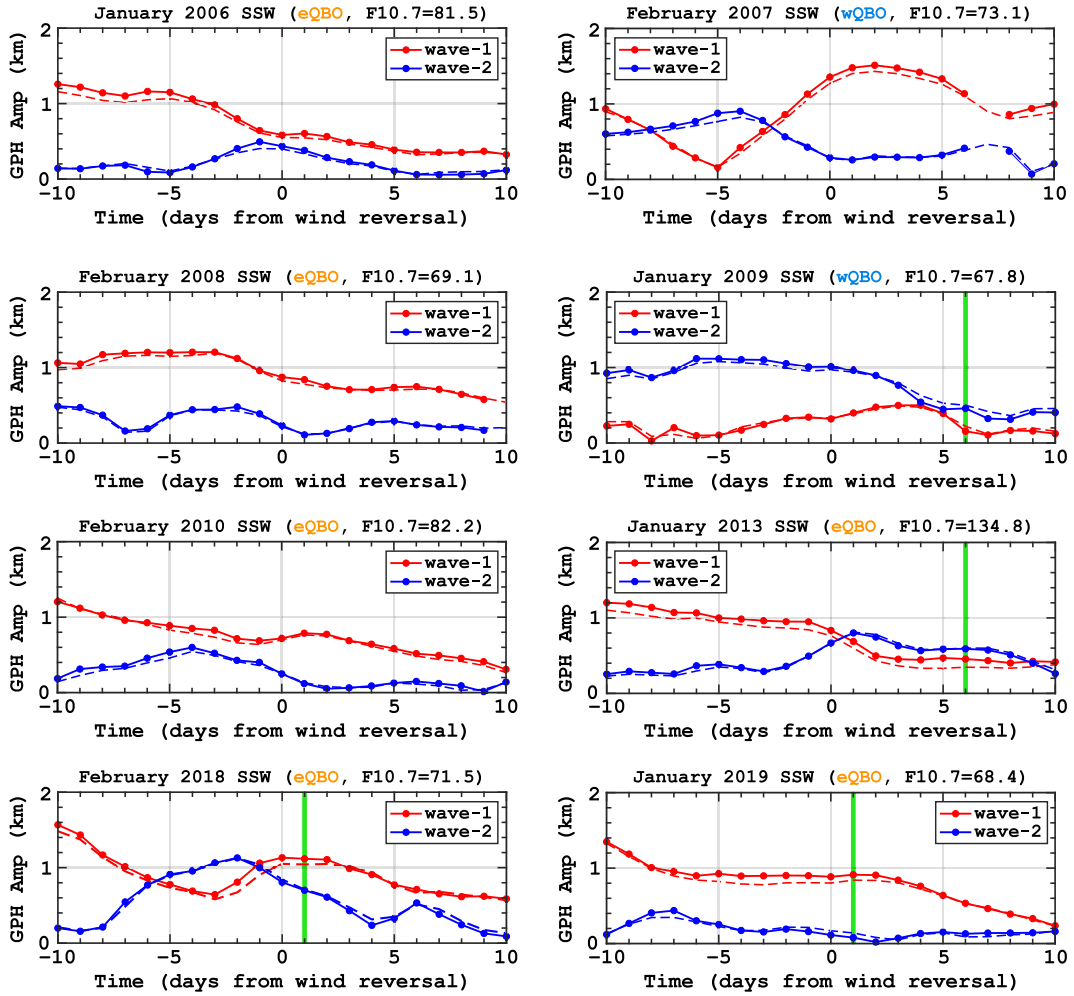


Figure 10. Overview of major sudden stratospheric warmings (SSW) observed during 2005–2020. Red and blue lines show daily amplitudes of wave-1 and wave-2 planetary waves at 60°N at 10 hPa, respectively. Solid lines correspond to amplitudes derived from Aura/MLS geopotential height (GPH) data, while dashed lines are the same but from the NCEP-DOE Reanalysis 2. Vertical green lines indicate the central date of quasi-4-day wave enhancement. Phase of the quasi-biennial oscillation (QBO) is indicated for each SSW. eQBO and wQBO correspond to easterly and westerly phases of the QBO, which are determined by the equatorial zonal wind at 50 hPa from the NCEP-DOE Reanalysis 2 averaged over ± 10 days from the day of the zonal wind reversal at 60°N at 10 hPa. The solar flux index $F_{10.7}$ averaged over the same time interval is also indicated for each SSW. The dates of wind reversal are 21 January 2006, 22 February 2007, 22 February 2008, 24 January 2009, 8 February 2010, 7 January 2013, 12 February 2018, and 31 December 2018.